Tribology International 126 (2018) 49–64

Contents lists available at ScienceDirect

Tribology International

journal homepage: www.elsevier.com/locate/triboint

Analysis of lubricating characteristics of valve plate pair of a piston pump

Zhaoqiang Wang[a,*], Shan Hu[a], Hong Ji[b], Zhen Wang[a], Xintian Liu[a]

[a] Automotive Engineering College, Shanghai University of Engineering Science Shanghai, 201620, China
[b] School of Fluid Power and Control Engineering, Lanzhou University of Technology, Lanzhou, 730050, China

ARTICLE INFO

Keywords:
Valve plate pair
Friction
Hydrodynamic
Temperature

ABSTRACT

The wedge-shaped oil film thickness, pressure and temperature distribution of the valve plate pair of an axial piston pump were investigated using finite difference and relaxation iterative methods and lubrication characteristics for different working conditions and tilt and non-tilt states of the cylinder block were analysed for comparison. The oil film thickness changed when the cylinder block was tilted relative to the valve plate and produced hydrodynamic effects, increasing the carrying capacity. The structural parameter of the valve plate pair influenced lubrication characteristics. The temperature of the oil film increased and the temperature field was unevenly distributed owing to frictional power–related changes to heat energy. The simulated temperature and friction coefficient showed good agreement with measured values.

1. Introduction

An axial piston pump is an important component of the hydraulic system of construction machinery and is widely used under severe conditions, as it can operate with high efficiency at high pressures and at various speeds [1,2]. The efficiency of a piston pump is relatively low at low speed because of insufficient lubrication. The interface between the cylinder block and valve plate represents one of the most critical design elements in the rotating kit of an axial piston pump [3–5].

The valve plate pair of a swash-plate axial piston pump is composed of the kidney-shaped slot of the valve plate, sealing clearance, and cylinder block. Its structural parameters affects the service life of axial piston pump [6–8]; a cylinder block within a high-speed pump is more likely to tilt away from the valve plate, which results in a wedge-shaped oil film between the valve plate and the cylinder block [9]. The tilting inertia moment on the cylinder block produced by the inertia forces of the piston/valve plate assemblies should be considered when analysing the cylinder block balance. A large tilting inertia moment will make the cylinder block tilt away from the valve plate, resulting in severe wear [10,11]. The valve plate pair undergoes friction that affects the efficiency of the axial piston pump, and the sealing volume varies with the reciprocating movement of the axial piston pump, thus realising the oil absorption and drainage process [12,13].

Many studies have investigated the hydrodynamic effects of the valve plate, but research on the temperature field of the valve plate pair has been scarce. Yamaguchi was the first person to introduce numerical methods in the calculation of the oil film pressure distribution of the axial piston pump, obtaining the law of pressure distribution in the seal belt [14–17]. Deng calculated the pressure of the valve plate pair and undertook the numerical analysis using the finite difference method [18]. Wang derived the formula for determining the pressure of the valve plate pair based on the Reynolds equation: the pressure and temperature field distribution of oil film were numerically analysed [19]. Wu derived the flow and the formula for the pressure in the sealing region of the port plate pair based on the Reynolds equation for disk gap and obtained the applicable linearization condition for the pressure distribution according to the calculation accuracy. The group also analysed the fields of pressure, speed, and temperature numerically using CFD (Computational Fluid Dynamics) software [20,21]. Ahn used the finite element method for the computation of the pressure distribution between a cylinder block and a valve plate of the axial piston pump [22]. Bergada clarified the understanding of the complex dynamics, pointing out how the oil film thickness depends on the oil pressure and temperature. Improvement of the efficiency of piston pumps could be a major step toward their development [23]. Kazama and Tsuruno measured the temperature of bearing/seal parts of axial piston pumps: the temperature of the swash plate between the crescent-shaped discharge and suction ports and that of the cylinder block at the bottom centre of the pistons increased markedly when the discharge pressure and rotational speed increased. The temperature rise was larger when the fluid viscosity was higher and the inlet oil temperature was lower [24]. Rybicki and Strenkowski presented a finite element numerical solution technique for compliant bearing lubrication. The mechanics of the compliant bearing surfaces is obtained from a finite

* Corresponding author. Vehicle Engineering Automotive Engineering College, Shanghai University of Engineering Science, China.
E-mail addresses: wangzhaoqiang_2008@sues.edu.cn (Z. Wang), 15317652575@163.com (S. Hu), jihong@lut.cn (H. Ji), wangzhenhello@126.com (Z. Wang), xintianster@gmail.com (X. Liu).

https://doi.org/10.1016/j.triboint.2018.05.008
Received 6 February 2018; Received in revised form 19 April 2018; Accepted 4 May 2018
Available online 07 May 2018
0301-679X/

Nomenclature

h	Thickness of oil film (m)	Φ	Dissipative work terms
h_0	Initial oil film thickness ($0.0325{\cdot}10^{-3}m$)	P	Lubricant pressure (Pa)
h_1	Minimum oil film thickness (m)	η	Viscosity of lubricating oil ($Pa{\cdot}s$)
h_2	Maximum oil film thickness (m)	η_0	Initial viscosity of oil film ($\eta_0 = 0.036572\,Pa\,s$)
R	Radius of one point on the oil film (m)	θ	Circumferential angle at a point (°)
R_1	Inner diameter of interior sealing belt ($0.0298\,m$)	ω	Cylinder block speed ($3000\,rpm$)
R_2	Outside diameter of interior sealing belt (m)	φ	Cylinder block tilt angle ($0.0004°$)
R_3	Inner diameter of outer sealing belt (m)	H	Width of the sealing belt ($0.0121\,m$)
R_4	Outside diameter of outer sealing belt ($0.0419\,m$)	F	Carrying capacity (N)
ω	Average stiffness of oil film(N/m)	T	Offset load torque ($N{\cdot}m$)
M_f	Friction torque (N/m)	Ff	Friction force (N)
ρ	Lubricating oil density	f	Friction coefficient
ρ_0	Lubricating oil density at a temperature of $T_0(890\,kg/m^3)$	C_ρ	Specific heat of lubricating oil(C_ρ = 870 J/kg/k)
k	Thermal conductivity of lubricant	α_T	Thermal expansion coefficient of lubricating oil ($°C^{-1}$)
J	Mechanical equivalent of heat ($4.184\,J/cal$)	$T_{i,j}$	Temperature (°C)
		T_0	The initial temperature (303 °C)
		β	Viscosity-temperature coefficient ($0.03°C^{-1}$)

element model. The mechanics of the fluid lubricant can be described by Reynold's equation. Coupling the behaviour of the fluid lubricant and compliant surfaces gives a set of non-linear equations [25]. Mucchi and Gazzi proposed an experimental methodology for analysis of the lubrication regime and wear that occurs between vanes and the pressure ring in variable displacement vane pumps. The lubrication regime is essential for the improvement of the performance of high-pressure vane pumps for reducing the wear, increasing the volumetric efficiency, and decreasing maintenance costs. Low wear and reduced friction can be obtained if elasto-hydrodynamic lubrication between vanes and pressure ring is established [26].

In this study, the oil film thickness, pressure, and temperature distribution were obtained by the finite difference method. The mathematical modelling of the valve plate was meshed, and the pressure value at each node constituted the difference quotient, approximating the derivative of the Reynolds equation and improving the accuracy of calculation [27,28]. The equation was reduced to a set of algebraic equations, the pressure values at each node were determined, a set of discrete pressure values were calculated, and the pressure distribution in the oil film was approximately obtained [29,30]. The cylinder block–valve plate contact model was based on the numerical solution of the generalized Reynolds equation and energy equations. The lubrication characteristics of different working conditions and two states of the cylinder block (tilt and non-tilt) were analysed for comparison and the optimal value was obtained.

Additionally, the frictional power changes to heat energy caused the temperature of the oil film and the temperature field to increase with uneven distribution. Experiments investigating the friction and temperature were carried out using a thermocouple and a micro-displacement sensor to verify the simulation results. Such an overall analytical approach has not hitherto been reported in literature. Thus, this work lays a foundation for the production of a axial piston pump with good performance and improved practical application of a friction pair to improve the service life of a piston pump.

2. Mathematical model of the valve plate pair

2.1. Model building

Fig. 1 shows the mathematical model of the valve plate pair with a tilt cylinder block: Fig. 1a is an assembly sketch of the cylinder block and valve plate; Fig. 1b is a representation of the valve plate with points of temperature measurement marked. The cylinder block was tilted relative to the valve plate and rotated in the anticlockwise direction. The oil film in the contact area between the valve plate and the cylinder block was ring-shaped [31–33].

On account of the oil film in the contact area was ring-shaped. Converting the rectangular coordinate system into polar coordinate system, the following is obtained.

$$\begin{cases} x=r\theta,\ \frac{\partial}{\partial x}=\frac{1}{r}\frac{\partial}{\partial \theta} \\ y=r,\ \frac{\partial}{\partial y}=\frac{\partial}{\partial \theta} \\ z=z,\ \frac{\partial}{\partial z}=\frac{\partial}{\partial z} \end{cases} \tag{2-1}$$

Reynolds equation is based on the assumption that the oil is adsorbed on the valve plate pair. The two-dimensional polar coordinates-based Reynolds equation can be simplified as follows [34]:

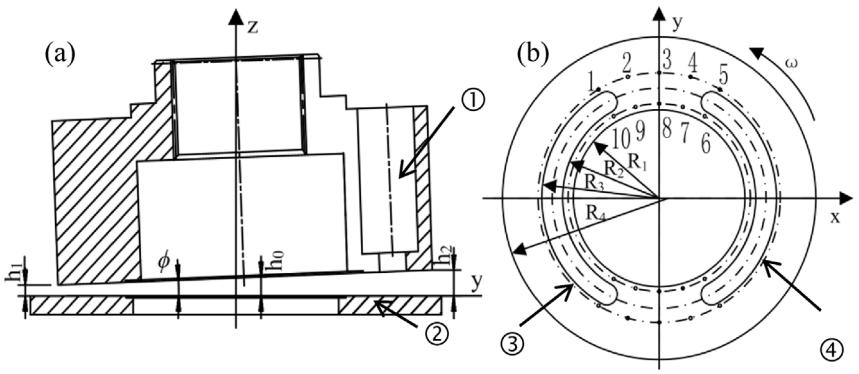

Fig. 1. Mathematical model of valve plate pair for piston pump, (a) assembly sketch of the cylinder block and valve plate, (b) representation of the valve plate with points of temperature measurement marked. (1) cylinder block, (2) valve plate, (3) high-pressure chamber, (4) low-pressure chamber.

$$\frac{\partial}{\partial r}\left(\frac{rh^3}{\mu}\frac{\partial p}{\partial r}\right)+\frac{1}{r}\frac{\partial}{\partial \theta}\left(\frac{h^3}{\mu}\frac{\partial p}{\partial \theta}\right)=6\ \omega\ r\frac{\partial h}{\partial \theta} \tag{2-2}$$

$6\ \omega\ r^{\partial h/\partial\theta}$ represents the shear flow caused by rotation of the cylinder block; $^{\partial/\partial r}\left(rh^{3}/\mu\cdot^{\partial p/\partial r}\right)$ refers to the differential pressure flow generated by the pressure gradient along the radial direction; $^{1/r\,\partial/\partial\theta}\left(h^{3}/\mu^{\partial p/\partial\theta}\right)$ represents the differential pressure flow generated by the pressure gradient along the angular direction.

2.2. Mathematical model assumption

The following assumptions were made for the oil film of the valve plate pair [35]:

(1) The effect of gravity was neglected;
(2) The lubricant oil was a Newtonian fluid;
(3) No slip existed on the surface of the cylinder block and the valve plate;
(4) The inertia force, body force, and temperature were neglected;
(5) The lubricating oil was an incompressible fluid;
(6) No elastic deformation existed on the surface of the cylinder block and the valve plate;
(7) Curvature of the valve plate end face had no effect on the results.

2.3. Discretization of the model

The accuracy of the full-differential form adopted was high, discretization along the X and Y directions was undertaken using the following [36]:

$$\left[\frac{\partial}{\partial r}\left(\frac{rh^3}{\mu}\frac{\partial p}{\partial r}\right)\right]_{i,j}+\left[\frac{1}{r}\frac{\partial}{\partial\theta}\left(\frac{h^3}{\mu}\frac{\partial p}{\partial\theta}\right)\right]_{i,j}=\left[6\omega\ r\frac{\partial h}{\partial\theta}\right]_{i,j} \tag{2-3}$$

Discretization:

$$\mathrm{P}_{i,j}=\frac{\mathrm{A}P_{i,j}+\mathrm{B}P_{i-1,j}+\mathrm{C}P_{i,j+1}+\mathrm{D}P_{i,j-1}-F}{E} \tag{2-4}$$

Where:

$$\mathrm{A}=\frac{r_{i+0.5,j}h^3}{\mu\Delta r^2} \tag{2-5}$$

$$\mathrm{B}=\frac{r_{i-0.5,j}h^3}{\mu\Delta r^2} \tag{2-6}$$

$$\mathrm{C}=\frac{1}{r_{i,j}}\frac{h^3}{\mu\Delta\theta^2} \tag{2-7}$$

$$\mathrm{D}=\frac{1}{r_{i,j}}\frac{h^3}{\mu\Delta\theta^2} \tag{2-8}$$

$$E=A+B+C+D \tag{2-9}$$

$$\mathrm{F}=6\omega r_{i,j}\frac{h_{i,j+0.5}-h_{i,j-0.5}}{\Delta\theta} \tag{2-10}$$

2.4. Decision criteria for the relative precision

According to the convergence condition of pressure, the iterative calculation will stop when the computational error satisfies the set of calculation accuracy and otherwise continue to calculate, with the strict criterion being that the pressure of all nodes satisfies the relative accuracy.

$$\left|\frac{P_{i,j}^{k+1}-P_{i,j}^{k}}{P_{i,j}^{k+1}}\right|\le\varepsilon_1 \tag{2-11}$$

Following assumption:

$$\mathrm{gap}=\frac{\sum_{i=2}^{n}\sum_{i=2}^{m}(P_{i,j}^{k+1}-P_{i,j}^{k})}{\sum_{i=2}^{n}\sum_{i=2}^{m}(P_{i,j}^{k+1})} \tag{2-12}$$

The criteria for judging convergence aregap ≤ err and accuracy error err = 10^{-4}.

2.5. Boundary condition

The initial pressure for the sealing belt of the valve plate pair was regarded as atmospheric pressure: $P_0 = 0.101325\,MPa$; The high-pressure oil port of the kidney-shaped slot determined the actual working condition pressure; The low-pressure oil port of the kidney-shaped slot determined the atmospheric pressure.

$$\begin{aligned}&P(r=r_1,\theta)=P_0\\&P(r=r_4,\theta)=P_0\\&P(r_2\le r\le r_3,\ 196^\circ\le\theta\le 344^\circ)=P\\&P(r_2\le r\le r3,\ 16^\circ\le\theta\le 164^\circ)=P_0\end{aligned} \tag{2-13}$$

The working surface of the valve plate was ring-shaped and the cycle conditions were at $0^\circ C$ and $360^\circ C$ [37]:

$$\begin{aligned}&P(r,2\pi)=P(r,0)\\&H(r,2\pi)=H(r,0)\end{aligned} \tag{2-14}$$

2.6. Program block diagram

The over-relaxation iteration method was adopted to reduce the computational complexity and shorten the computation time. Fig. 2 shows the program block diagram of calculation.

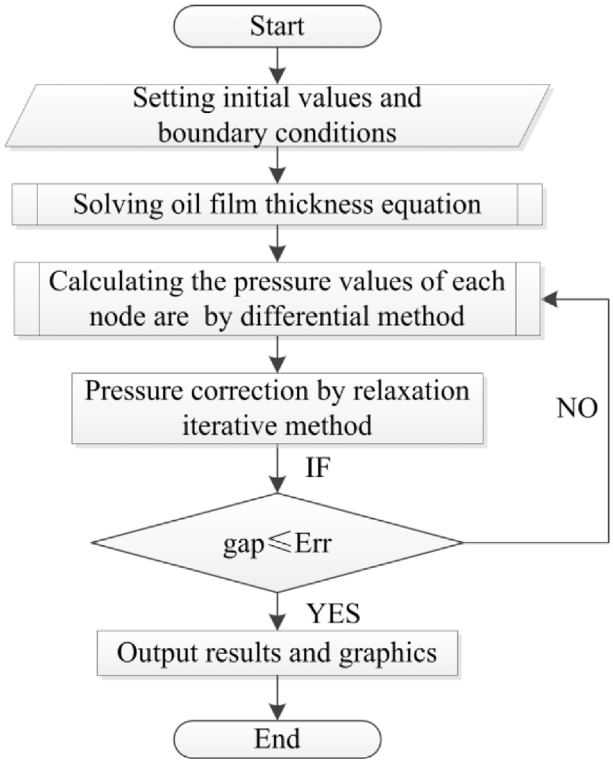

Fig. 2. Program block diagram of calculation.

3. Oil film morphology and the pressure distribution nephogram

The tribological mechanism between the valve plate and the cylinder block in oil hydraulic axial piston pumps plays an important role in determining the high power density [38,39].

3.1. Oil film thickness distribution

If a straight line is drawn perpendicular to the valve plate, meeting the valve plate at one point and the cylinder block at another point, the length between the two points is the thickness of the oil film. The equation used to determine the oil film thickness equation is as follows:

$$h_{i,j} = h_0 + r_{i,j}\sin(\theta_{i,j})\tan\varphi \tag{3-1}$$

The film thickness equation follows the radial direction, where the forward and backward central difference equation is:

$$h_{i+0.5,j} = h_0 + r_{i+0.5,j}\sin(\theta_{i+0.5,j})\tan\varphi \tag{3-2}$$

Fig. 3 shows the distribution of the oil film thickness: the thickness of the wedge-shaped oil film varies with the inclination of the cylinder block. The oil film thickness is thicker at the top and thinner below, and there is no oil film in the middle.

3.2. Oil film pressure distribution

The distribution of the oil film pressure is nonlinear in the sealing belt, which creates the offset load torque and causes dynamic changes to the wedge-shaped oil film [40]. Fig. 4 shows that the distribution of the oil film pressure does not consider the high-pressure oil port: the opening direction of the wedge-shaped oil film remains unchanged when the working condition parameter does not vary, and the thickness of the oil film in the low-pressure zone is larger.

Fig. 5 shows the distribution of the oil film pressure considering the high-pressure: the pressure value was set at 35 *MPa*; the lower side represents the low-pressure oil port of the kidney-shaped slot, which was set as the atmospheric pressure, and the upper side represents the high-pressure oil port, which was set as the working pressure. High-pressure is produced for a lower thickness of the wedge-shaped oil film with rotation of the cylinder block, and the oil film pressure gradually rises with an increasing angle and then decreases to 0. The oil film pressure rises gradually in the upper and lower dead centre region as the radius increases.

4. Maximum pressure and minimum oil film thickness of the valve plate pair at different parameters

4.1. Effect of cylinder block speed on maximum pressure and minimum oil film thickness

Fig. 6 shows the variation of the maximum pressure and minimum thickness caused by changes in the speed: as the speed increased from 1000 rpm to 6000 rpm, the maximum pressure increased from 101338.3Pa to 161187.6Pa, whereas the minimum oil film thickness was 2.957483e −5*m* and remained the same.

Fig. 7 shows the oil film pressure distribution at different rotational speeds: the speed increased from 3000 rpm to 6000 rpm, and the pressure distribution of the valve plate pair oil film increased with increasing speed.

4.2. Effect of the tilt angle of cylinder block on maximum pressure and minimum oil film thickness

Fig. 8 shows the variation of the maximum pressure and minimum thickness caused by changes to the tilt angle: as the angle increased from 0.001° to 0.01°, the maximum pressure increased from 101334.7Pa to 161187.6Pa, and the minimum oil film thickness decreased from 3.1768708e−5m to 2.5187072e −5*m*.

Fig. 9 shows the oil film pressure distribution at different inclination angles; the pressure distribution of the valve plate pair oil film increased with increase in the angle.

4.3. Effect of initial oil film thickness on maximum pressure and minimum oil film thickness

Fig. 10 shows the variation of the maximum pressure and minimum thickness owing to changes in the initial oil film thickness: as the initial oil film thickness increased from 1.e−6m to 5. e−5m, the maximum pressure decreased from 54293608Pa to 101335.8Pa and the minimum oil film thickness increased from 2.07483e −6m to 4. 707483e −5m.

Fig. 11 shows the oil film pressure variation distribution at different initial oil film thicknesses. The pressure distribution of the valve plate pair decreased with increasing initial oil film thickness.

4.4. Effect of lubricating oil viscosity on maximum pressure and minimum oil film thickness

Fig. 12 shows variation of the maximum pressure and minimum thickness caused by changes in the viscosity: as the viscosity increased from 0.01 Pa·s to 0.1 Pa·s, the maximum pressure increased from 101336 *Pa* to 218068.9 *Pa* and the minimum oil film thickness was

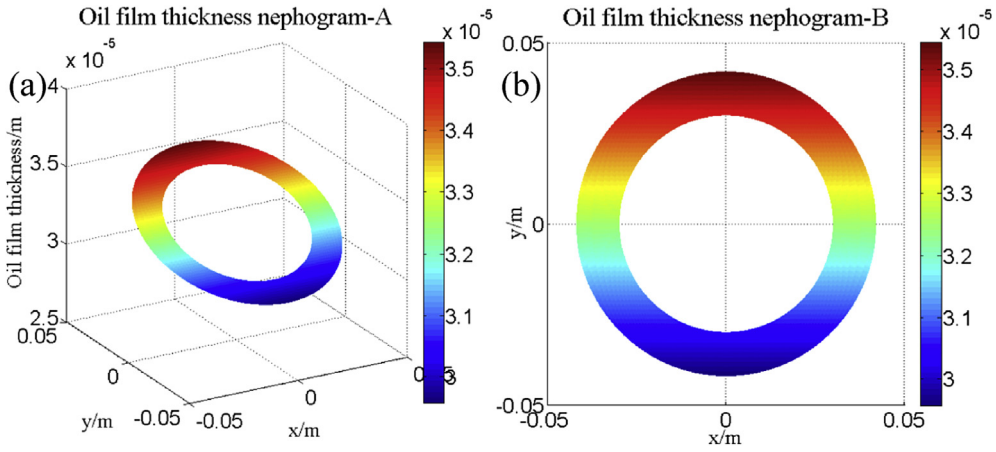

Fig. 3. The distribution of the oil film thickness, (a) 3D diagram of the oil film distribution and (b) top view of the wedge oil film thickness.

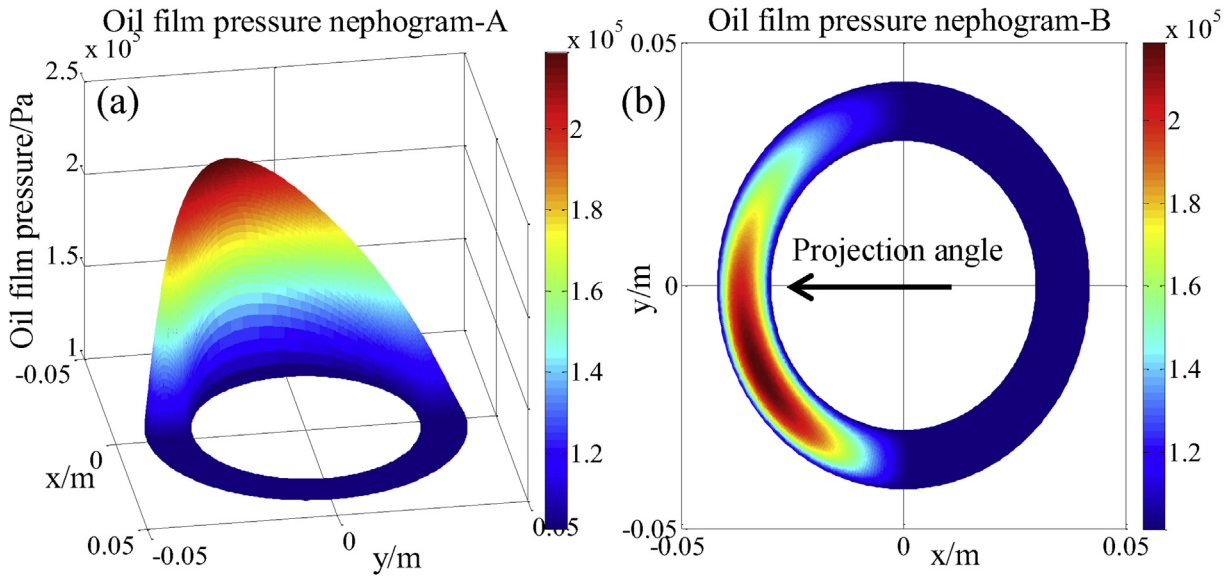

Fig. 4. The distribution of oil film pressure does not consider the high-pressure oil port, (a) 3D diagram of the pressure distribution, (b) top view of the pressure distribution.

2.957483e−5 m and remained the same.

Fig. 13 shows the variation of pressure caused by changes in the lubricating oil viscosity: as the latter increased from 0.03pa·*s* to 0.06pa·*s*, the pressure distribution of the oil film increased.

4.5. Effect of the sealing belt width on maximum pressure and minimum oil film thickness

Fig. 14 shows the variation of the maximum pressure and minimum thickness because of changes in the sealing belt width: as the width increased from 0.011 *m* to 0.017 *m*, the maximum pressure increased from 101357.4Pa to 163438.8Pa and the minimum thickness decreased from2.9651623e−5m to 2.9232744e−5m.

Fig. 15 shows the variation of the maximum pressure caused by changes in the sealing belt width: as the width increased from 0.012 *m* to 0.015 *m*, the pressure of the valve plate pair increased.

5. Lubricating characteristics of the valve plate pair at different parameters

The pressure according to Reynolds equation is related to the speed of the cylinder block, the viscosity, and the oil film thickness. The oil film thickness is in turn related to the initial oil film thickness and the tilt angle of the cylinder block. Reynolds equation is derived from the Navier-Stokes equations, which is the basis of hydrodynamic lubrication and reflects the load-carrying capacity. The lubricating characteristics (carrying capacity, offset load torque, friction force, friction torque, friction coefficient, and average stiffness of oil film) of the valve plate pair were determined as the structural parameters (speed, viscosity, angle of cylinder block tilting and initial oil film thickness) were changed to obtain a comparative analysis.

Carrying capacity:

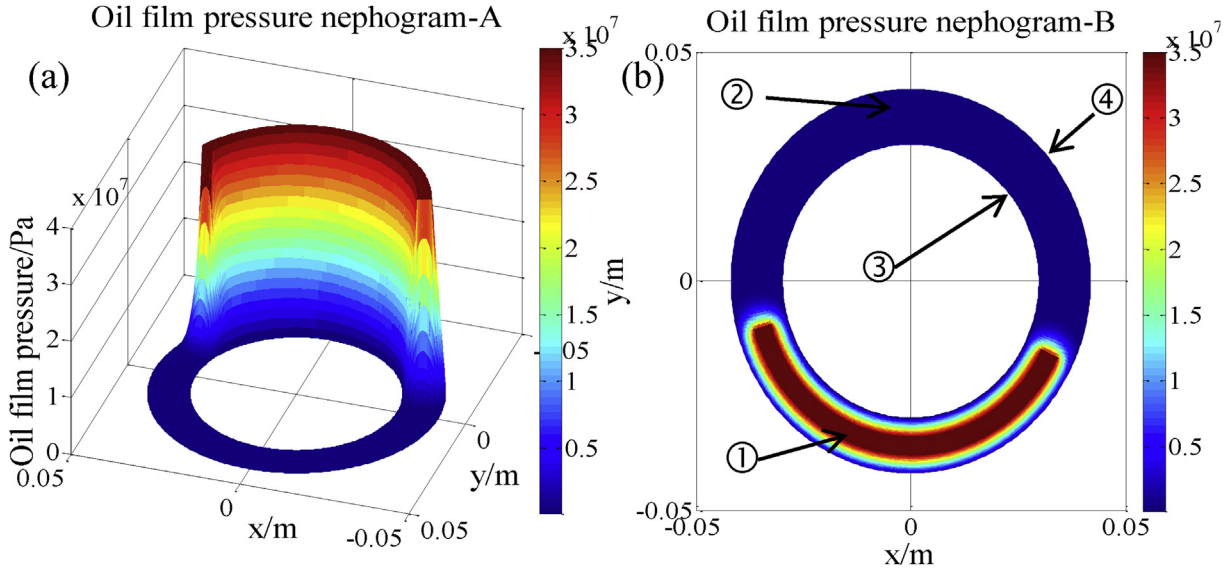

Fig. 5. Oil film pressure distribution consider the high-pressure kidney-shaped slot, (a) 3D diagram of the oil film pressure distribution, (b) top view of the oil film pressure distribution. (1) high-pressure oil port, (2) low-pressure oil port, (3) inner sealing belt, (4) outer sealing belt.

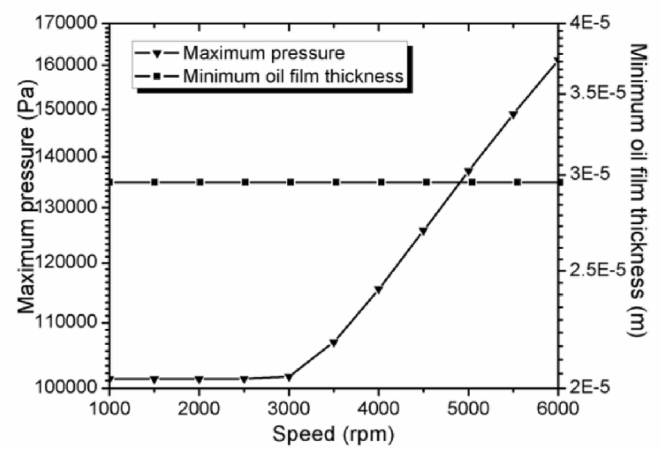

Fig. 6. The effect of speed on maximum pressure and minimum oil film thickness.

$$F=\sum_{i=1}^{n}\sum_{j=1}^{m}P_{i,j}r_{i,j}\Delta\theta\Delta r \tag{5-1}$$

Offset load torque:

$$M_x=\sum_{i=1}^{n}\sum_{j=1}^{m}P_{i,j}r_{i,j}\sin(\theta_{i,j}))\Delta\theta\Delta r$$
$$M_y=\sum_{i=1}^{n}\sum_{j=1}^{m}P_{i,j}r_{i,j}\cos(\theta_{i,j}))\Delta\theta\Delta r \tag{5-2}$$

Resultant torque:

$$T=\sqrt{(M_x)^2+(M_y)^2} \tag{5-3}$$

Average stiffness of oil film:

$$w=\frac{F}{h_0} \tag{5-4}$$

Friction force:

$$F_f=\sum_{i=1}^{n}\sum_{j=1}^{m}\mu\omega\frac{r_{i,j}}{h_{i,j}}\Delta\theta\Delta r \tag{5-5}$$

Friction torque:

$$M_f=\sum_{i=1}^{n}\sum_{j=1}^{m}\mu\omega\frac{r_{i,j}}{h_{i,j}}\Delta\theta\Delta r \tag{5-6}$$

Friction coefficient:

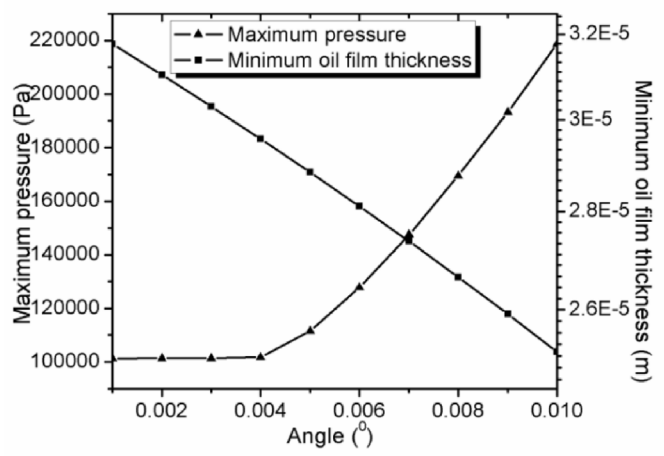

Fig. 8. The effect of angle on maximum pressure and minimum oil film thickness.

$$f=\frac{F_f}{F} \tag{5-7}$$

5.1. Effect of cylinder block speed on lubricating characteristics

Fig. 16 shows determination of the valve plate pair structure parameters: as the speed increased from 500 rpm to 5000 rpm, the lubricating characteristics changed under different scenarios as follows.

5.1.1. Tilt of cylinder block considered

The carrying capacity increased from 303.0258 *N* to 303.1432 *N*; the offset load torque decreased from 8.140716 *N* to 8.140374 *N*; the friction force increased from 7.098662e −2 *N* to 7.09891e −1 *N*; the friction torque increased from 2.594257e −3*N·m* to 2.594258e −2 *N·m*; the friction coefficient increased from 2.3425937e −4 to 2.3417673e −3; the average stiffness of the oil film increased from 9323869 *N/m* to 9327483 *N/m*.

5.1.2. Tilt of cylinder block not considered

The carrying capacity was 303.039 *N* and remained the same; the offset load torque was 8.138518 *N* and remained the same; the friction force increased from 7.0986621e −2*N* to 7.098908e −1*N*; the friction torque increased from 2.5942565e −3*N·m* to 2.5942575e −2*N·m*; the friction coefficient increased from 2.3424912e−4 to 2.3425724e−3; the average stiffness of the oil film was 9324277*N*/mand remained the same.

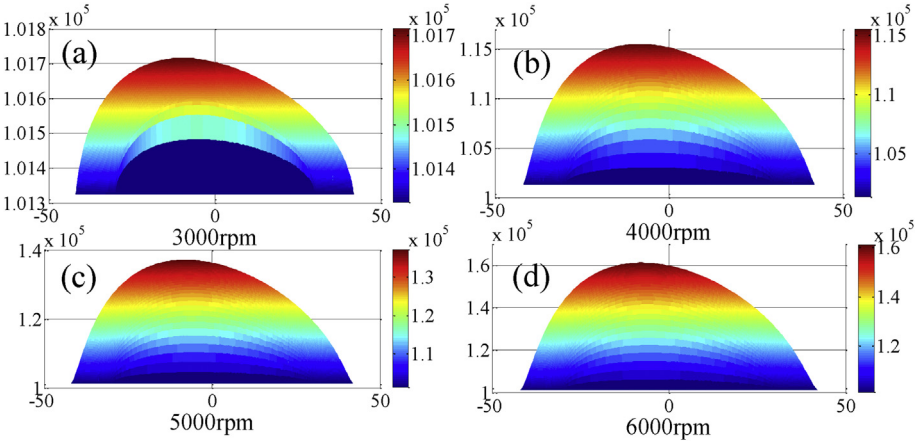

Fig. 7. Oil film pressure variation distribution at different rotational speeds, (a) speed of the cylinder block was 3000 rpm, (b) speed was 4000 rpm, (c) speed was 5000 rpm, (d) speed was 6000 rpm.

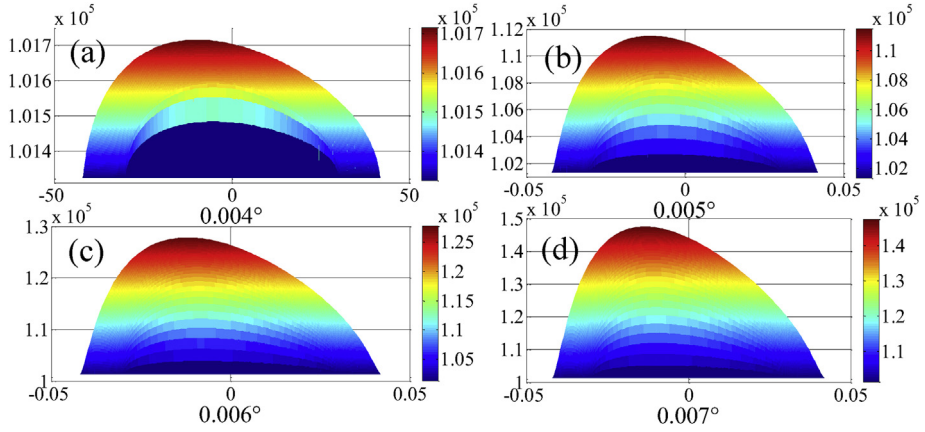

Fig. 9. Oil film pressure variation distribution at different inclination angles, (a) angle is 0.004°, (b) angle is 0.005°, (c) angle is 0.006°, (d) angle is 0.007°.

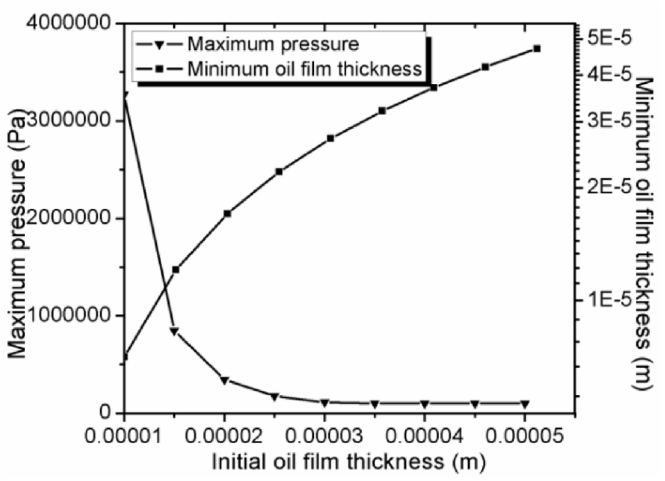

Fig. 10. The effect of initial oil film thickness on maximum pressure and minimum oil film thickness.

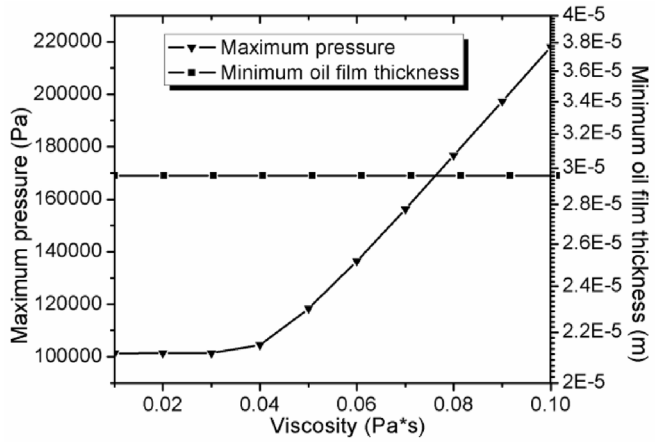

Fig. 12. The effect of initial oil film thickness on maximum pressure and minimum oil film thickness.

5.2. *Effect of lubricating oil film viscosity on lubricating characteristics*

Fig. 17 represents determination of the valve plate pair structure parameters: as the viscosity increased from 0.01*Pa·s* to 0.1*Pa·s*, the lubricating characteristics changed as follows under different scenarios.

5.2.1. *Tilt of cylinder block considered*

The carrying capacity increased from 303.0317 *N* to 303.2094 *N*; the offset load torque decreased from 8.140642 *N* 8.139678 *N*; the friction force increased from 0.1176557 *N* to 1.176607 *N*; The friction torque increases from 4.2999559e −3 *N·m* to 4.2998869e−2*N·m*; the friction coefficient increased from 3.8826195e−4 to 3.8805099e−3; the average stiffness of the oil film increased from 9324053*N*/m to 9329521*N*/m.

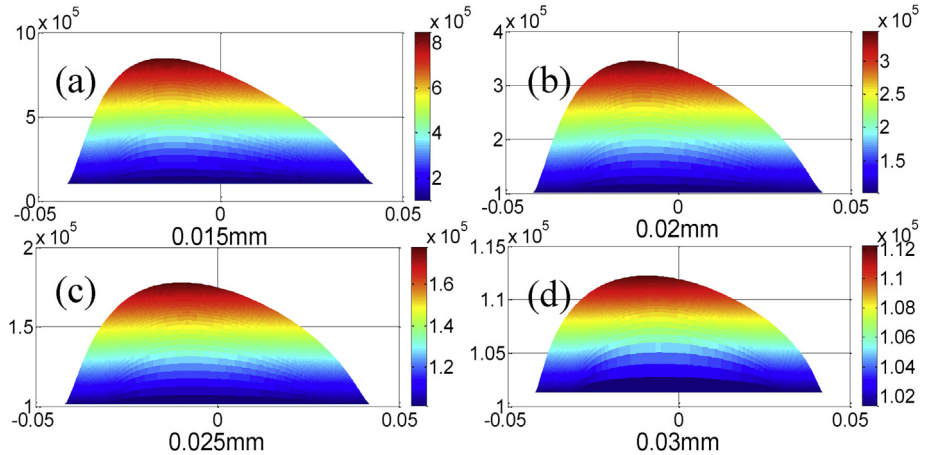

Fig. 11. Oil film pressure variation distribution at different initial oil film thickness (a) thickness is 0.015 mm, (b) thickness is 0.020 mm, (c) thickness is 0.025 mm, (d) thickness is 0.030 mm.

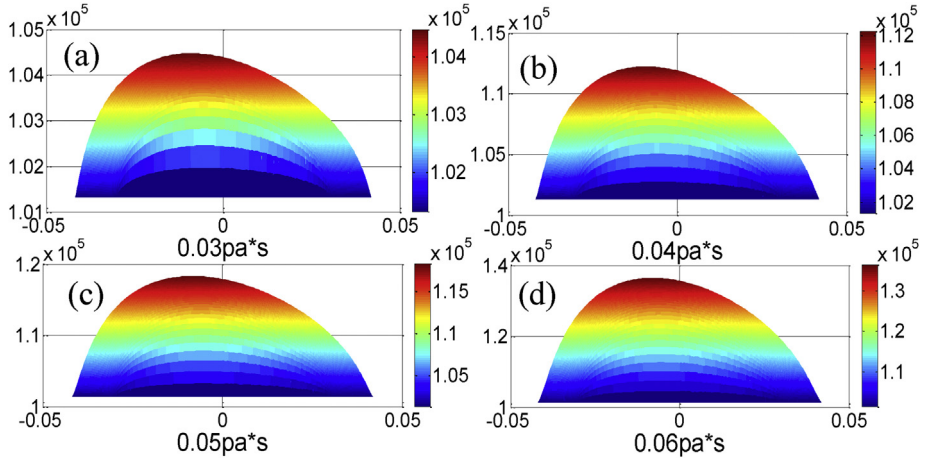

Fig. 13. Oil film pressure distribution at different lubricating oil viscosities, (a) viscosity is 0.03pa·*s*, (b) viscosity is 0.04pa·*s*, (c) viscosity is 0.05pa·*s*, (d) viscosity is 0.06pa·*s*.

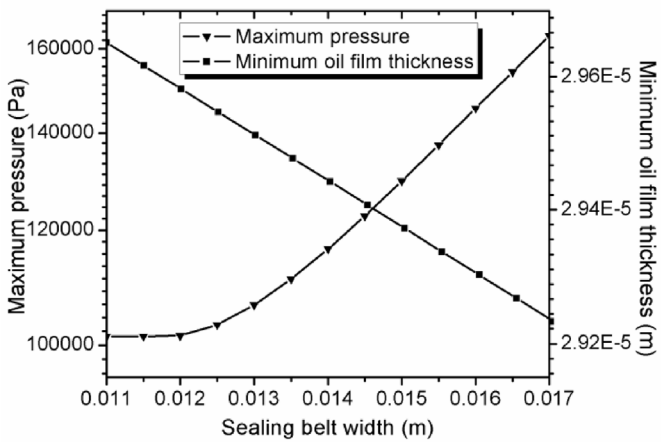

Fig. 14. The effect of sealing belt width on maximum pressure and minimum oil film thickness.

5.2.2. Tilt of cylinder block not considered

The carrying capacity was 303.039 *N* and remained the same; the offset load torque was 8.138518 *N·m* and remained the same; the friction force increased from 0.1176557 *N* to 1.176607 *N*; the friction torque increased from 4. 3000115e−4*N·m* to 4. 2999559e−3 *N·m*; the friction coefficient increased from 3.8824699e−5 to 3.8825261e−4; the average stiffness of the oil film was 932427.9*N*/mand remained the same.

5.3. Effect of cylinder block inclination angle on lubricating characteristics

Fig. 18 represents the determined valve plate pair structure parameters: as the tilt angle increased from 0.001° to 0.01°, the lubricating characteristics changed as follows under different scenarios.

5.3.1. Tilt of cylinder block considered

The carrying capacity increased from 303.052 *N* to 303.0737 *N*; the offset load torque increased from 0.425898 *N* to 8.140122 *N*; the friction force was 0.425898 *N* and remained the same; the friction torque was 1.5565805e−2 *N·m* and remained the same; the friction coefficient decreased from 1.4053627e−3 to 1.4047815e−4; the average stiffness of the oil film increased from 9324676*N*/m to 9325344*N*/m.

5.4. Effect of initial film thickness on lubricating characteristics

Fig. 19 shows the determined valve plate pair structure parameters: as the initial oil film thickness increased from 1.e−5*m* to 1.e−4*m*, the lubricating characteristics changed as follows under different scenarios.

5.4.1. Tilt of cylinder block considered

The carrying capacity decreased from 305.373 *N* to303.0402 *N*; the offset load torque increased from 8.139211 *N* to 8.141141 *N* when the initial oil film thickness was 2e−5*m* then decreased from 8.141141*N* to 8.139359*N*; the friction force decreased from 1.384254 *N* to0.138421 *N*; the friction torque decreased from 5.05895e −2 *N·m* to5.0588544e−3 *N·m*

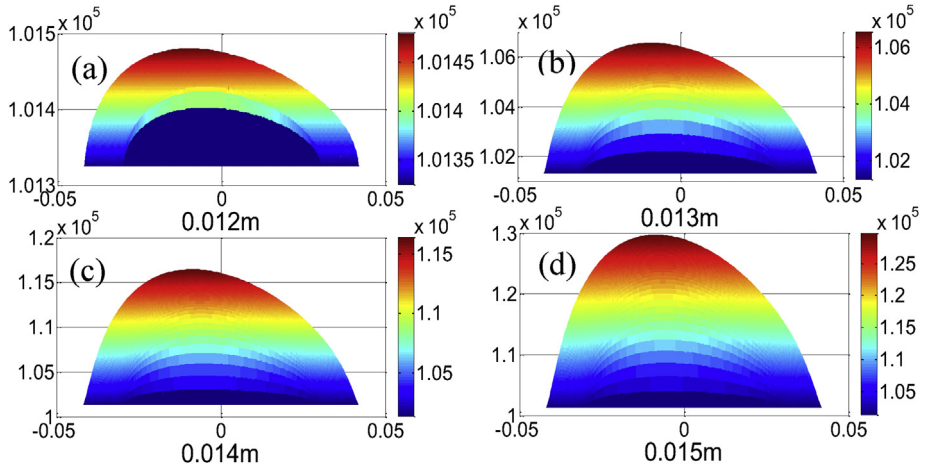

Fig. 15. Oil film pressure distribution at different sealing belt width, (a) sealing belt width is 0.012 *m*, (b) width is 0.013 *m*, (c) width is 0.014 *m*, (d) width is 0.015 *m*.

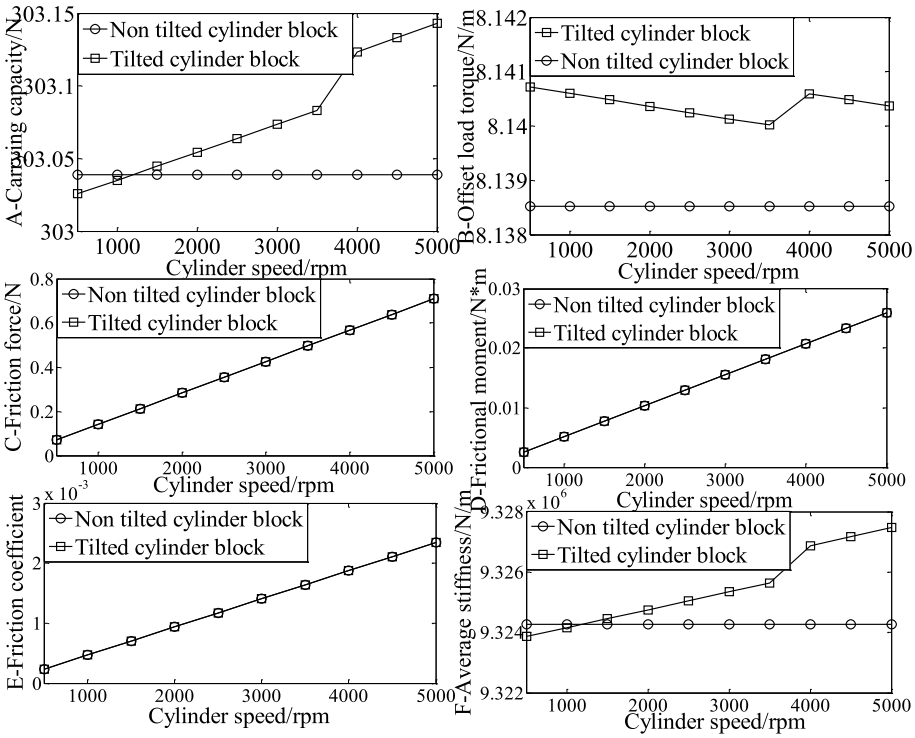

Fig. 16. The effect of cylinder block's speed on lubricating characteristics, (A) carrying capacity, (B) offset load torque, (C) friction force, (D) friction torque, (E) friction coefficient, (F) average stiffness of oil film.

; the friction coefficient decreased from 4.5329952e −3 to 4.5677563e −4; the average stiffness of the oil film decreased from 30537300N/m to 3030402N/m.

5.4.2. Tilt of cylinder block not considered

The carrying capacity was 303.039 $N$and remained the same; the offset load torque was 8.138518$N{\cdot}m$and remained the same; the friction force decreased from 1.384254 N to 0.138421 N; the friction torque decreased from 5. 058948e−2$N{\cdot}m$ to 5.0588544e−3$N{\cdot}m$; the friction coefficient decreased from 4.5679077e −3 to 4.5677784e −4; the average stiffness of the oil film decreased from 3. 03039 e7N/m to 3.030387 e6N/m.

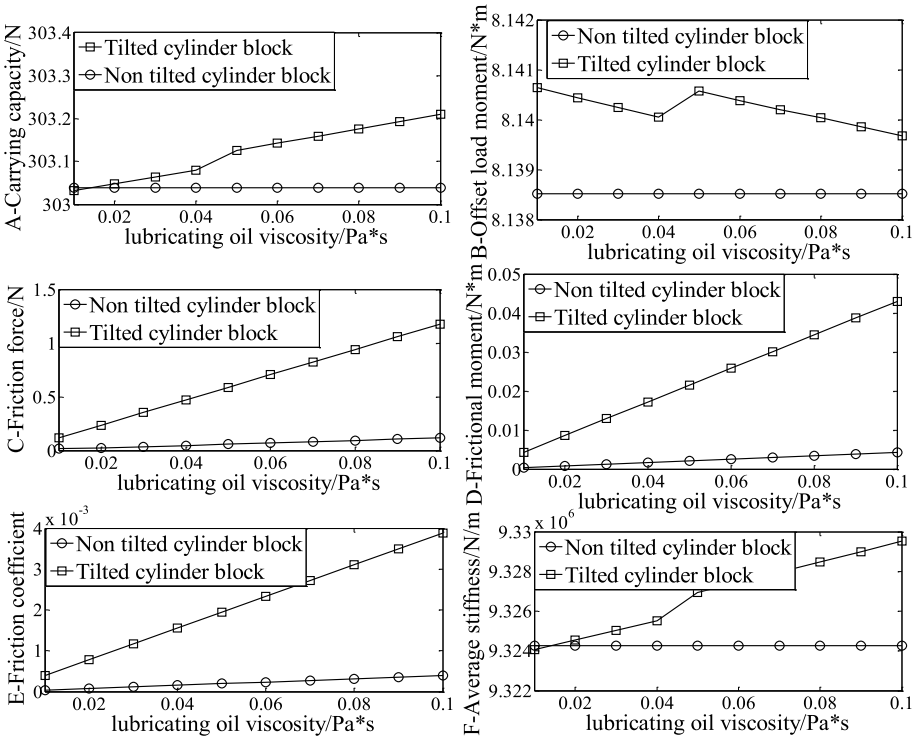

Fig. 17. The effect of lubricating oil film viscosity on lubricating characteristics, (A) carrying capacity, (B) offset load torque and (C) friction force, (D) friction torque, (E) friction coefficient, (F) average stiffness of oil film.

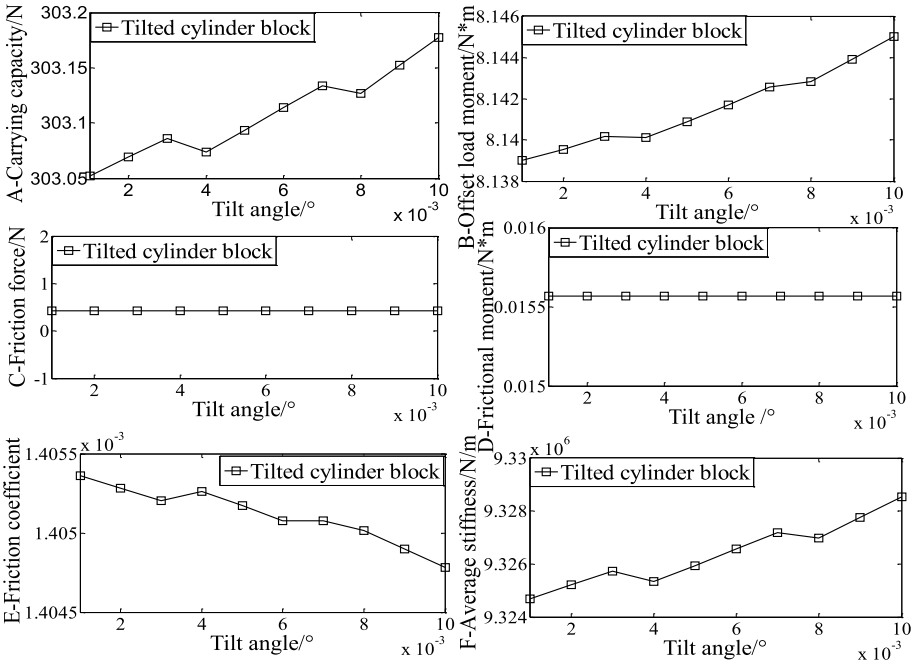

Fig. 18. Effect of tilting angle on lubricating characteristics, (A) carrying capacity and (B) offset load torque and (C) friction force and (D) friction torque and (E) friction coefficient and (F) average stiffness of oil film.

5.5. Effect of sealing belt width on lubricating characteristics

Fig. 20 exhibits the determined valve plate pair structure parameters: as the sealing belt width increased from 0.011 *m* to 0.016 *m*, the lubricating characteristics changed as follows.

5.5.1. Tilt of cylinder block considered

The carrying capacity decreased from 253.571 *N* to 501.1352 *N*; the offset load torque increased from 6.77865 *N* to 13.63912 *N*; the friction force increased from 0.340801 *N* to 0.83253 *N*; the friction torque decreased from 1.22292e −2 *N·m* to 3.24266 e−2*N·m*; the friction coefficient decreased from 1.344003 e−3 to 1.66130 e−3; the average stiffness of the oil film decreased from 7802197*N*/m to 15419545 *N*/m.

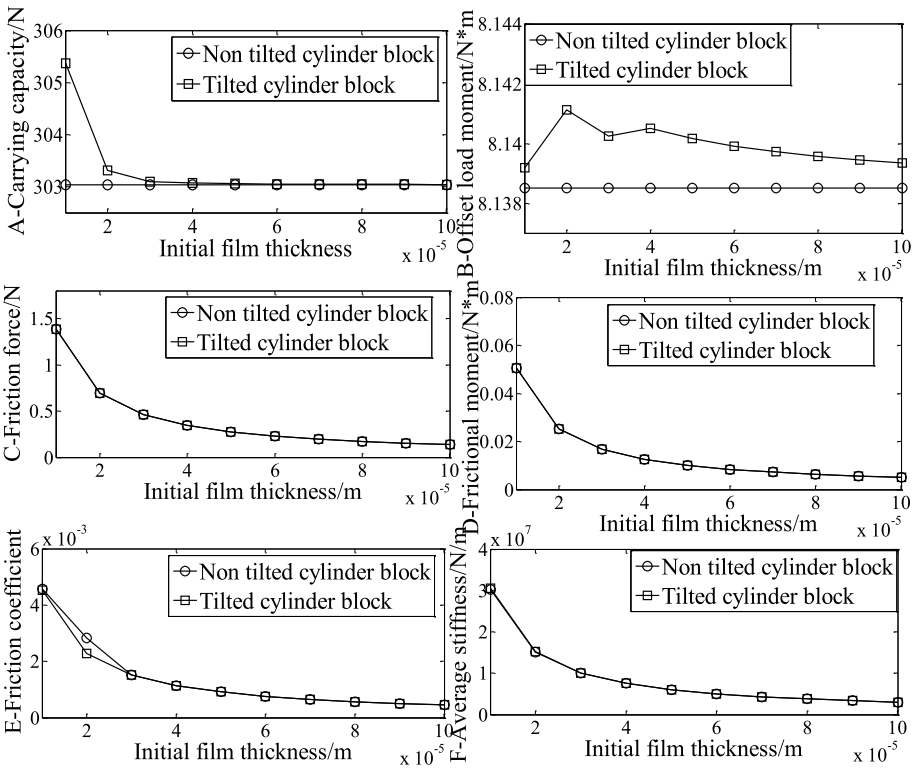

Fig. 19. Effect of initial film thickness on lubricating characteristics, (A) carrying capacity, (B) offset load torque, (C) friction force, (D) friction torque, (E) friction coefficient, (F) average stiffness of oil film.

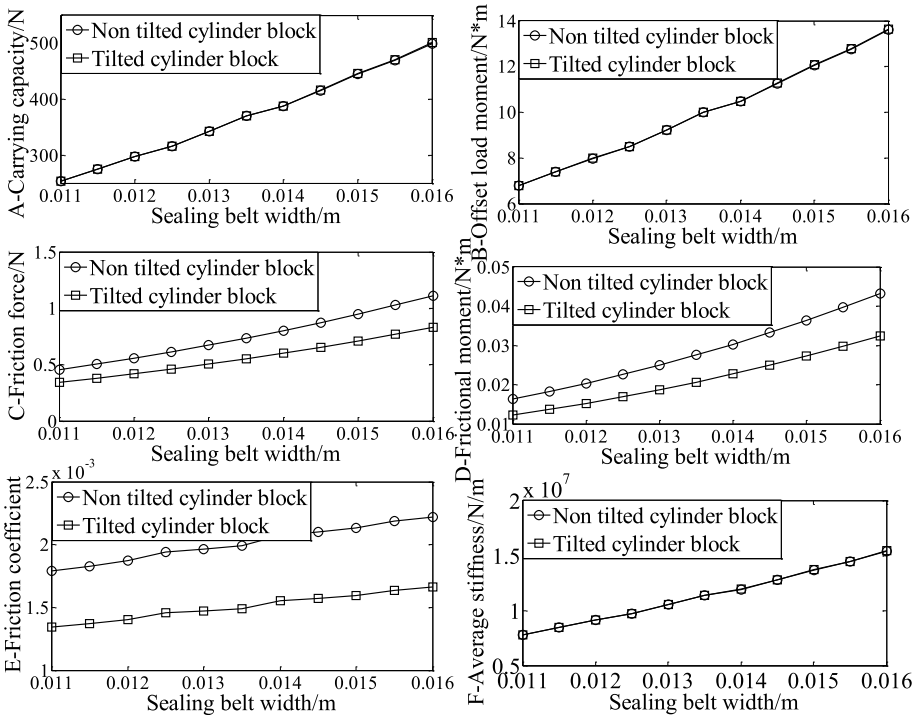

Fig. 20. The effect of sealing belt width on lubricating characteristics, (A) carrying capacity, (B) offset load torque, (C) friction force, (D) friction torque, (E) friction coefficient, (F) average stiffness of oil film.

5.5.2. Tilt of cylinder block not considered

The carrying capacity increased from 253.7024 *N* to 499.6635 *N*; the offset load torque increased from 6.78116 *N·m* to 13.60076 *N·m*; the friction force increased from 0.4543865 *N* to 1.110096 *N*; the friction torque increased from 1. 630627 e−2*N·m* to 4.3233395e−2*N·m*; the friction coefficient increased from 1.791022 e−3 to 2.22169 e−3; the average stiffness of the oil film increased from 7. 80623 e6*N*/m to 1. 537423e7 *N*/m.

5.6. Effect of high-pressure oil port pressure on lubricating characteristics

Fig. 21 shows the determined valve plate pair structure parameters: as the high-pressure oil port pressure increased from 5 *MPa* to 50 *MPa*, the lubricating characteristics changed as follows.

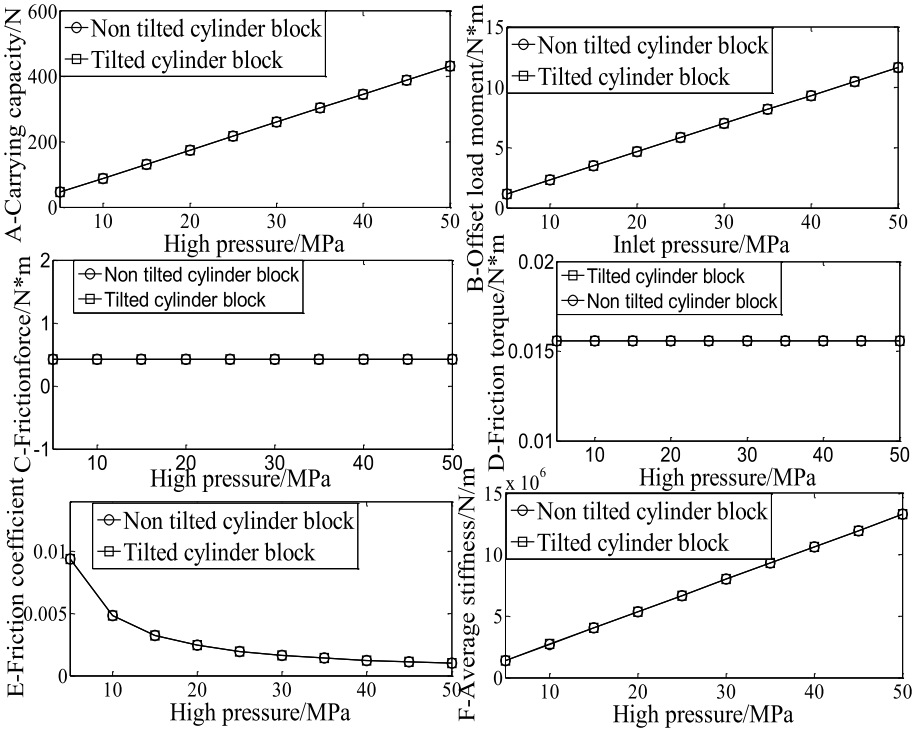

Fig. 21. The effect of high-pressure oil on lubricating characteristics, (A) carrying capacity, (B) offset load torque, (C) friction force, (D) friction torque, (E) friction coefficient, (F) average stiffness of oil film.

5.6.1. Tilt of cylinder block considered

The carrying capacity decreased from 45.44472 N to 431.8925 N; The offset load torque increased from 1.140289 N 11.6402 N; the friction force was 0.425898 N and remained the same; the friction torque was 15565805e −2$N{\cdot}m$ and remained the same; the friction coefficient decreased from 9.3717817e −3 to 9.8612043e−4; the average stiffness of the oil film decreased from 1398299 N/m to 13288999 N/m.

5.6.2. Tilt of cylinder block not considered

The carrying capacity increased from 45.37868 N to 431.8694 N; the offset load torque increased from 1.140414 N to 11.63755 N; the friction force was 0.425898 N and remained the same; the friction torque was 0.01556581 $N{\cdot}m$ and remained the same; the friction coefficient decreased from 9. 3854191e −2 to 9.8617317e−4; the average stiffness of the oil film increased from 1396267N/m to 13288288 N/m.

6. Oil film temperature distribution of valve plate pair

The valve plate pair is influenced by the lubricating oil viscosity during operation. Mechanical energy is consumed continuously by the oil film supplied by the cylinder block. The friction power changes to heat energy, causing the temperature of the oil film to increase and uneven distribution of the temperature field. Only part of the heat is taken up by the oil flow and some of it is also passed to the cylinder block and valve plate directly by the lubricant, which then spreads to the ambient medium. If the speed of cylinder and load of valve plate pair and oil supply condition remain unchanged, the friction heat, oil flow heat, and conduction dissipation reach a relatively stable state after a while of operation, and thus a stable temperature field is established.

A representation of the valve plate with points of temperature measurement marked was shown in Fig. 1b.

6.1. Energy equation

The results obtained using Reynolds equation agreed with the pressure calculation when calculating the temperature. The general energy equation is as follows:

$$\mathrm{JC}_\rho\left(\mu\frac{\partial T}{\partial x}+\upsilon\frac{\partial T}{\partial y}+\omega\frac{\partial T}{\partial z}\right)=k\left(\frac{\partial^2 T}{\partial x^2}+\frac{\partial^2 T}{\partial y^2}+\frac{\partial^2 T}{\partial z^2}\right)-\frac{T}{\rho}\frac{\partial \rho}{\partial T}\left(\mu\frac{\partial p}{\partial x}+\upsilon\frac{\partial \mathrm{p}}{\partial y}+\omega\frac{\partial p}{\partial z}\right)+\Phi \tag{6-1}$$

The main factors influencing the temperature are as follows:

(1) Temperature variation is inversely proportional to the oil film thickness: the maximum temperature occurs for the minimum film thickness and the lowest temperature is recorded for the maximum oil film thickness;
(2) Temperature increase is proportional to $\left({}^{\partial p}/_{\partial x}\right)^2$ and inversely proportional to $\left({}^{\partial p}/_{\partial y}\right)^2$.

6.2. Simplification of energy equation

Considering that the temperature, pressure, and viscosity did not change along the oil film thickness. The density of the lubricating oil is independent of the temperature. The energy equation commonly used in hydrodynamic lubrication is as follows:

$$q_x\frac{\partial \mathrm{T}}{\partial x}+q_y\frac{\partial \mathrm{T}}{\partial y}=\frac{\eta U^2}{J\rho c_\rho h}+\frac{h^3}{12\eta J\rho c_\rho}\left[\left(\frac{\partial p}{\partial x}\right)^2+\left(\frac{\partial p}{\partial y}\right)^2\right] \tag{6-2}$$

Where: $q_x=\frac{Uh}{2}-\frac{h^3}{12\eta}\frac{\partial p}{\partial x}$; $q_y=-\frac{h^3}{12\eta}\frac{\partial p}{\partial y}$.

Consistent with the process used for determining the pressure, cylindrical polar coordinates were used in this case, as well. Equations (6-2) can also be expressed as Eqs (6-3):

$$\mathrm{J}\rho\mathrm{C}_\rho\left[\left(\frac{r\omega h}{2}-\frac{h^3}{12\mu}\frac{\partial P}{r\partial\theta}\right)\frac{\partial T}{r\partial\theta}-\frac{h^3}{12\mu}\frac{\partial P}{\partial r}\frac{\partial T}{\partial r}\right]=\frac{\mu}{\mathrm{h}}(\omega r)^2+\frac{h^3}{12\mu}\left[\left(\frac{\partial P}{r\partial\theta}\right)^2+\left(\frac{\partial P}{\partial r}\right)^2\right] \tag{6-3}$$

6.3. Difference of energy equation

The energy equation is discretized by dimensions, and the formula (6-3) is transformed:

$$\frac{\partial T}{\partial\theta}=\frac{r}{\mathrm{Q}_x}\left(\frac{Q_y\frac{\partial T}{\partial r}+\frac{\mu}{\mathrm{h}}(\omega r)^2+\frac{h^3}{12\mu}\left[\left(\frac{\partial P}{r\partial\theta}\right)^2+\left(\frac{\partial P}{\partial r}\right)^2\right]}{\mathrm{JC}_\rho\rho}\right) \tag{6-4}$$

Formula deformation:

$$\mathrm{A}_1=\mathrm{JC}_\rho\rho \tag{6-5}$$

$$B_1=\frac{\mu_{i,j}}{\mathrm{h}_{i,j}}(\omega r_{i,j})^2+\frac{h_{i,j}}{12\mu_{i,j}}\left[\left(\frac{\partial P}{r_{i,j}\partial\theta}\right)^2+\left(\frac{\partial P}{\partial r}\right)^2\right] \tag{6-6}$$

$$\mathrm{C}_1=\frac{\Delta\theta}{\Delta r}r_{i,j}\frac{Q_y}{Q_x} \tag{6-7}$$

$$D_1=\frac{(\Delta\theta)}{\mathrm{Q}_x}r_{i,j} \tag{6-8}$$

$$E_1=T_{i,j}-C1\cdot T_{i,j-1} \tag{6-9}$$

$$\mathrm{Q}_x=\frac{Y_j\omega H_{i,j}}{2}-\frac{H_{i,j}}{12\eta_{i,j}}\frac{P_{i,j}-P_{i-1,j}}{\theta_i-\theta_{i-1}}$$
$$Q_y=\frac{H_{i,j}}{12\mu_{i,j}}\frac{P_{i,j}-P_{i,j-1}}{Y_i-Y_{i-1}} \tag{6-10}$$

$$T_{i,j}=\frac{\left(E_1+\frac{D_1\cdot B_1}{A_1}\right)}{1-C_1} \tag{6-11}$$

6.4. Viscosity–temperature equation

The Barus equation is usually adopted when attempting to determine the effect of temperature on viscosity:

$$\eta_{i,j}=\eta_0\exp[-\beta(T-T_0)] \tag{6-12}$$

viscosity–temperature equation:

$$\eta=\eta_0\exp\left\{\frac{(\ln\eta_0+9.67)}{\left[\left(\frac{T-138}{T_0-138}\right)^{-1.1}-1\right]}\right\} \tag{6-13}$$

6.5. Density–temperature equation

$$\rho=\rho_0[1-\alpha_T(T-T_0)] \tag{6-14}$$

The effect of temperature on viscosity is due to the increase in volume caused by thermal expansion, which leads to a decrease in the density. Generally, the effect of temperature on density is negligible.

6.6. Program block diagram and calculation steps

Calculation of the temperature uses the viscosity of the current node, which is directly affected by the current node temperature. Fig. 22 Shows the temperature calculation block diagram.

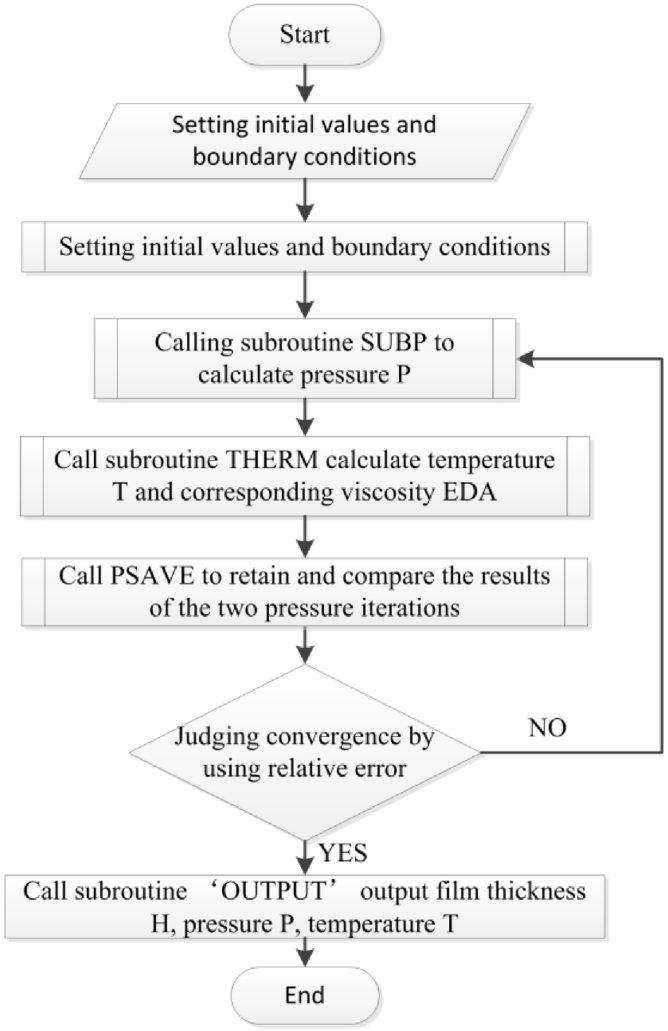

Fig. 22. Program flowchart of temperature calculation.

6.7. Friction and temperature test experiment

The friction coefficient refers to the ratio between the friction and vertical force on two surfaces and is related to the surface roughness [41]. The valve plate temperature is distributed within a certain range under certain working conditions; The central point of the valve plate is measured in order to study the effect of the piston pump working process on the valve plate temperature.

Fig. 23 shows the setup for testing the friction coefficient for the valve plate on CETR UMT-3 (Type of Rub Tester): the speed of the friction test machine increased from 50 rpm to 300 rpm during operation.

Fig. 24 shows the test curve for the friction coefficient for the valve plate on CETR UMT-3; Fig. 25 shows the test curve obtained for the friction coefficient for the valve plate as the pressure increased from 30 *N* to 110 *N*.

Fig. 26 shows the local diagram for an oil film temperature test device for the axial piston pump and data collection interface: deep holes were processed at the back of the sealing belts, and the distance from the valve plate oil film was 1 mm. The temperature at the upper central position of the distributor was measured. The initial and ambient temperature of the oil was 10°*C*; the piston pump was run for 5 min and then the measurements were begun.

Corresponding conditions are set as follows by setting two different inlet pressure values.

The pressure of oil inlet was first set to 10 *MPa*, the speed of cylinder block was set to 500 rpm, and the temperature of oil film was observed after waiting for 5 min. Then, the speed of cylinder block was set to 1000 rpm, the temperature of oil film was read after waiting for 5 min and the speed of cylinder block was allowed to rise to 1800 rpm, and the corresponding temperature of oil film was then recorded.

The pressure of oil inlet was set to 15 *MPa*, the speed of cylinder block was set to 1800 rpm and maintained, and the temperature of oil film was observed after waiting for 5 min. The pressure of oil inlet was retained, the speed of cylinder block was reduced to 1500 rpm, and the temperature of oil film was recorded after waiting for 5 min and the measurements were stopped when the speed of cylinder block dropped to 500 rpm.

Fig. 27 shows the measured valve plate temperature distribution: the speed was increased from 500 rpm to 1800 rpm and the working pressures were 10 *MPa* and 15 *MPa*; The temperatures at points 1 to 5 were higher than those at points 6 to 10; the temperature increased with increasing speed under the same pressure. Under the same conditions, the temperature at point 3 was slightly higher than that at points 1, 2, 4, and 5. Similarly, out of points 6 to 10, the temperature at point 8 was slightly higher than the other recorded values. This explains that the upper central oil starvation zone of the valve plate is a high-temperature point.

6.8. Temperature simulation calculation

Fig. 28 shows the oil film temperature distribution nephogram for the valve plate pair: the temperature near the high-pressure kidney-shaped slot was higher, the temperature gradient was large in direction of the film thickness, the lower temperature appeared in the region of the low-pressure kidney-shaped slot, and the temperatures in the upper and lower central regions (transition zone) were moderate.

Fig. 29 shows the temperature distribution curve obtained for the valve plate: the calculation angle ranged from 150° to 210° and the speed was increased from 500 rpm to 1800 rpm. The radius of the inner sealing belt was 31 *mm*, corresponding to the experimental location spanning points 6 to 10. The radius of the outer sealing belt was 40 *mm*, corresponding to the experimental location spanning points 1 to 5.

6.9. Comparison of measurements and calculations

In Figs. 27 and 29, the comparison of the curves obtained from

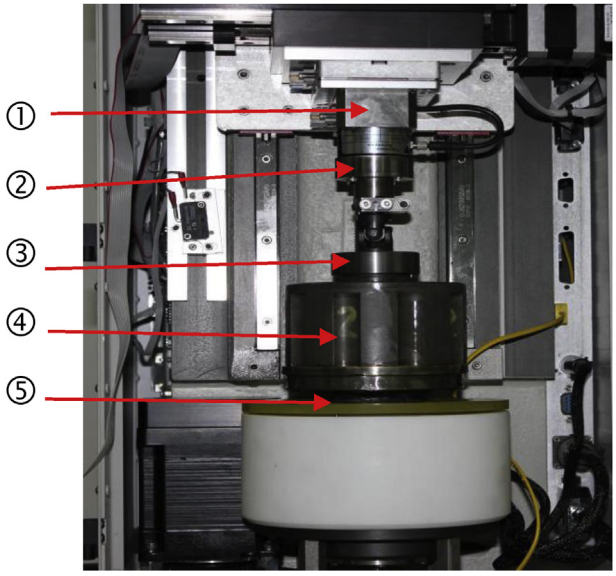

Fig. 23. Test of friction coefficient for valve plate on CETR UMT-3, (1) pin holder, (2) force sensor, (3) link holder, (4) cylinder block, (5) rotary table.

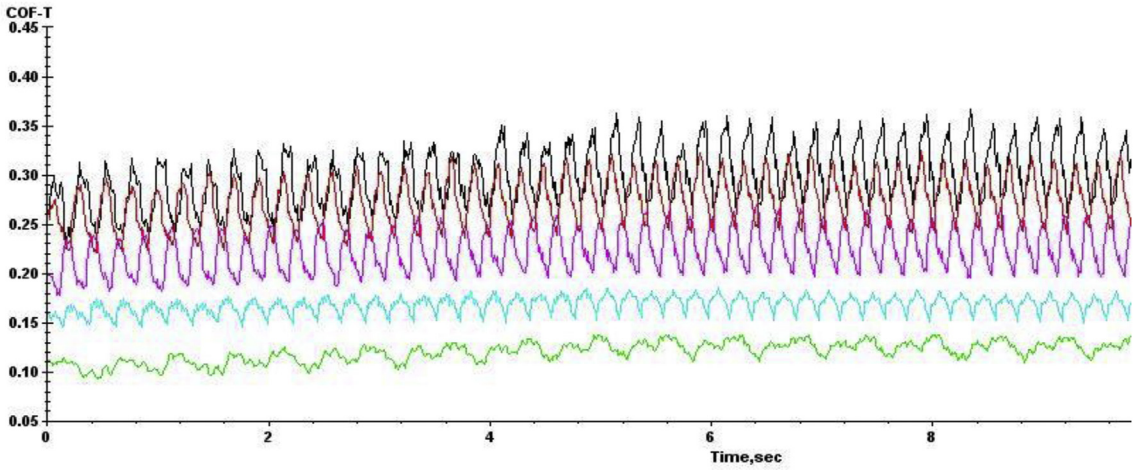

Fig. 24. Test curve of friction coefficient for valve plate on CETR UMT-3.

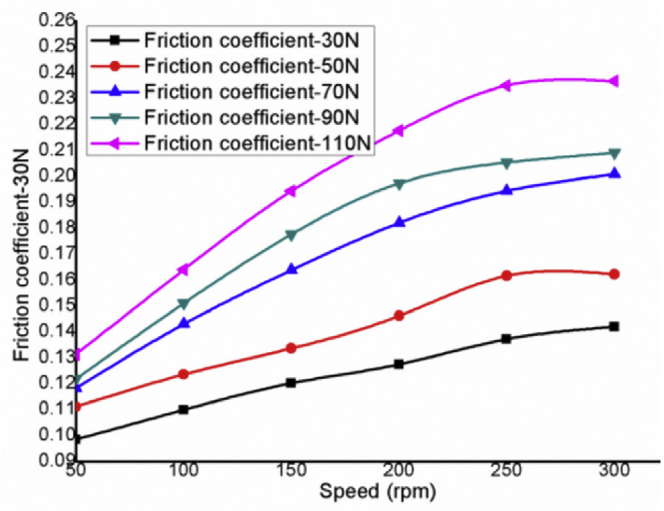

Fig. 25. Test curve of friction coefficient for valve plate.

measured and calculated temperature values for operation points 1 to 10 of the valve plate is illustrated. In addition to the temperature variation curve, the measured friction coefficient has been included. The calculated temperature and friction coefficient show good qualitative agreement with the measurements, and the agreement between measurements and calculations even increases for the sealing belt. In general, the calculated temperatures were relatively low compared to the measured results. This could be attributed to the fact that the piston pump in the experiment operated in a high-pressure oil field. The environment for experimental measurements was different, the experimental conditions cannot take into account all the factors. Furthermore, an additional damping effect was observed, which was not included in the simulation model. Nevertheless, the calculation model matched with the measured friction force well.

7. Conclusions

In this work, the oil film thickness, pressure, and temperature distribution were determined to investigate the lubrication characteristics of two states of the cylinder block (tilt and non-tilt) under different working conditions and the results were compared. Based on analytical and experimental results, the following conclusions may be drawn:

(1) The unbalanced force is generated by the high- and low-pressure chambers between the two sides of the valve plate; the wedge-shaped oil film is produced by the tilting of cylinder block relative to the valve plate, which can cause the hydrodynamic effect, improving the carrying capacity and friction force, and change the pressure distribution.
(2) The oil film pressure of the valve plate pair increased at the convergence region anticlockwise; the maximum pressure increased approximately linearly with increasing cylinder block speed, angle of inclination, and lubricant oil viscosity; the maximum pressure increased approximately linearly with decrease in the initial film thickness. The oil film thickness decreased with increase in the pressure and temperature during the simulations, and the temperature variation was approximately inversely proportional to the

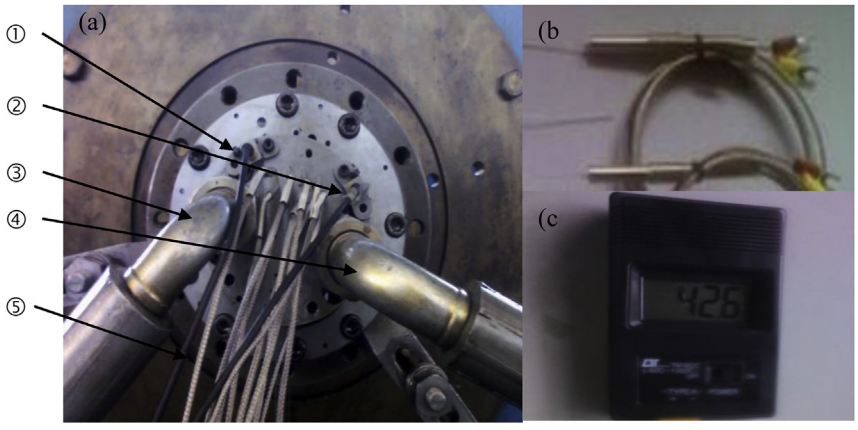

Fig. 26. Oil film temperature test device for axial piston pump, (a) local diagram of oil film temperature test device for axial piston pump, (b) superfine K type armored thermocouple, (c) datum thermocouple and display instrument. (1) micro displacement sensor 1, (2) micro displacement sensor 2, (3) oil out pipe, (4) oil inlet pipe, (5) thermocouple 1-10.

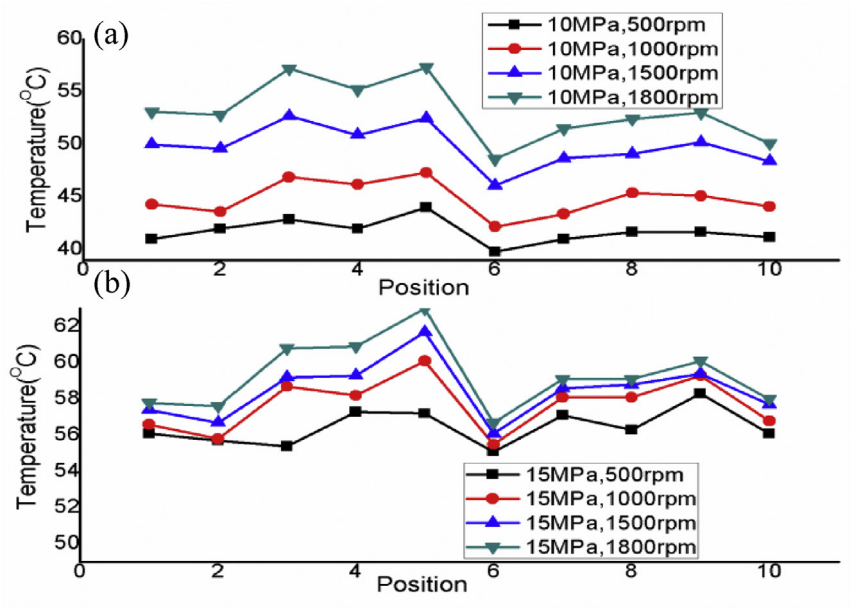

Fig. 27. Valve plate measured temperature distribution (a) working pressure is 10*Mpa*, (b) working pressure is 15 *MPa*.

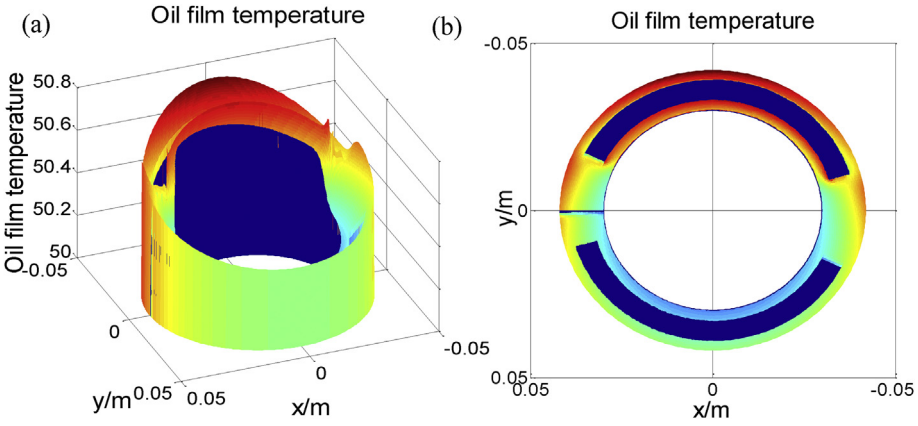

Fig. 28. Temperature distribution nephogram, (a) 3D diagram of the oil film temperature distribution, (b) top view of the oil film temperature distribution.

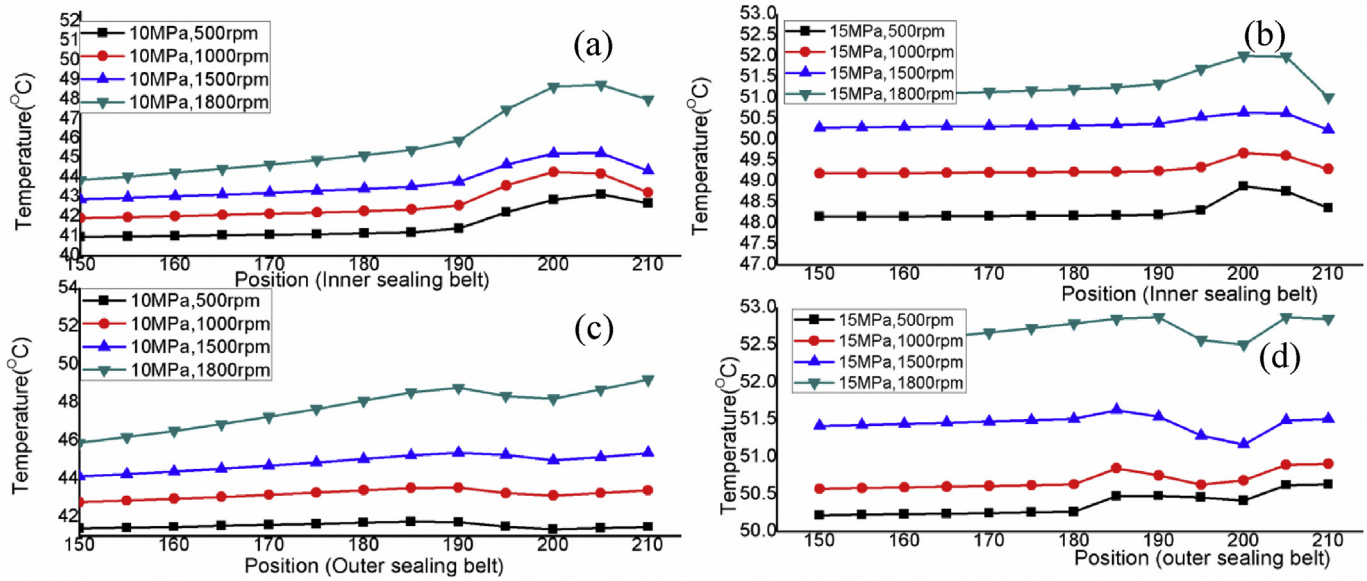

Fig. 29. Temperature distribution curve of valve plate, (a) work pressure is 10 *MPa* (inner sealing belt), (b) work pressure is 10 *MPa* (outer sealing belt), (c) work pressure is 15 *MPa* (inner sealing belt), and (d) work pressure is 15 *MPa* (outer sealing belt).

oil film thickness.

(3) The friction coefficient increased with increasing cylinder block speed, and the experimental results agreed with the observation. The maximum temperature was observed in the region of minimum oil film thickness, and the minimum temperature was observed in the region of maximum oil film thickness during the experiment. A smaller oil film thickness leads to greater shear stress and greater friction power loss, thus resulting in a greater temperature rise. The larger the radius under the same angular velocity, the higher is the linear velocity and the higher is the temperature rise, as confirmed by experimental results.

(4) The simulation predicted that the temperature of the oil film increased and the distribution of temperature field was uneven owing to the friction power changing to heat energy, which was similar to experimental results obtained. The temperature distribution of the oil film is an important factor that affects the lubrication performance, which can significantly change the viscosity of lubricating oils and consequently affect the pressure distribution and carrying capacity.

(5) The oil film temperature is also related to the structural parameters of the piston pump (sealing belt width and angle of inclination), working conditions parameters of the piston pump (cylinder speed and inlet pressure) and lubrication parameters of the oil film (viscosity and initial oil film thickness). However, further simulations and experimental verification are required to provide a theoretical basis for a high-speed and high-pressure piston pump. The calculated friction coefficient showed good qualitative and quantitative agreement with the measurements. A discrepancy noted between experimental and simulation results could have been caused by the restrictions imposed by the conditions used in the experiment, since the pump can only change the speed, lubricating oil viscosity, and inlet pressure during the experiment.

Acknowledgments

This study was funded by Project Nos. 51505272 and 51505274, supported by the National Natural Science Foundation of China and Project No. GZKF-201514, supported by the Open Foundation of the State Key Laboratory of Fluid Power and Mechatronic Systems.

References

[1] Shin JH, Kim HE, Kim KW. A study on models for the analysis of pressure pulsation in a swash-plate type axial piston pump. Am J Phys Anthropol 2011;27(6):503–18.
[2] Chao Q, Zhang J, Xu B, Chen Y, Ge YZ. Spline design for the cylinder block within a high-speed electro-hydrostatic actuator pump of aircraft. Meccanica 2018;53(1–2):395–411.
[3] Zhu Y, Chen X, Zou J. A study on the influence of surface topography on the low-speed tribological performance of port plates in axial piston pumps. Wear 2015;338–339:406–17.
[4] Koc E, Ng K, Hooke CJ. An analysis of the lubrication mechanisms of the bush-type bearings in high pressure pumps. Tribol Int 1997;30(8):553–60.
[5] Zecchi M. A Novel Fluid Structure Interaction and Thermal Model to Predict the Cylinder Block/Valve Plate Interface Performance in Swash Plate Type Axial Piston Machine Diss. Theses Gradworks 2013. p. 22–4.
[6] Wang S. Robust design of piston assemblies in an axial piston pump. Int J Fluid Power 2014;15(2):69–76.
[7] Ohno T, Azuma M. Valve Plate and axial piston hydraulic pump motor including the same. 2015. US9175672.
[8] Zloto T. Simulation of the hydrostatic load of the valve plate-cylinder block system in an axial piston pump. Procedia Eng. 2017;177:247–54.
[9] Chao Q, Zhang J, Xu B. Discussion on the Reynolds equation for the slipper bearing modeling in axial piston pumps. Tribol Int 2018;118:140–7.
[10] Zhang J, Chao Q, Xu B. Analysis of the cylinder block tilting inertia moment and its effect on the performance of high-speed electro-hydrostatic actuator pumps of aircraft. Chin J Aeronaut 2018;31(1):169–77.
[11] Kazama T. Numerical simulation of a slipper with retainer for axial piston pumps and motors under Swash Plate vibration vol. 10. 2017. p. 18–23. 2.
[12] Bae JH, Chung WJ, Jang JH. Study of pressure and flux pulsation to design optimum valve-plate notch and pulsation-variables analysis of swash-plate-Type piston pump. J. Korean Soc. Manuf. Technol. Eng. 2015;24(2):244–50.
[13] Zoto T, Nagórka A. Analysis of the pressure distribution of oil film in the variable height gap between the axial piston pump and cylinder block in the axial piston pump. Architectural Institute of Japan 2007:129–30.
[14] Yamaguchi A. Pressure distribution on valve plates of axial plunger pumps and motors. Prod. Res. 1966;18(7):186–8.
[15] Yamaguchi A. Formation of a fluid film between a valve plate and a cylinder block of piston pumps and motors: 2nd report, a valve plate with hydrostatic pads. Trans. Jpn. Soc. Mech. Eng. 1986;52(478):2412–7.
[16] Yamaguchi A, Sekine H, Shimizu S. Bearing/seal characteristics of the film between a valve plate and a cylinder block of axial piston pumps. Effects of fluid types and theoretical discussion. J Fluid Contr 1990;20(4):7–29.
[17] Yamaguchi A. Formation of A Film fluid between a valve plate and A Cylinder block of piston pumps and motors: 2nd report, a valve plate with hydrostatic pads. JSME International Journal Bulletin of the JSME 2008;30:87–92.
[18] Deng HS, Xu XL. Pressure analysis of a new type of axial piston pump's port plate pair with uniform flow. 2011.
[19] Wang B. Real-time measurement on lubrication characteristic parameters of plane port pair in axial piston pumps. Trans Chin Soc Agric Mach 2009;40(9):209–11.
[20] Wu ZD, Suo WX, Wang LQ. Analysis of the thermo-hydrodynamic lubrication performance of thrust bearings with water lubricated stationary pad. Large Electr Mach Hydraul Turbine 2001:14–8.
[21] Lin X, Jiang S, Zhang C. Thermohydrodynamic analysis of high speed water-lubricated spiral groove thrust bearing considering effects of cavitation, inertia and turbulence. Tribol Int 2018;119:645–58.
[22] Ahn SY, Rhim YC, Hong YS. Lubrication and dynamic characteristics of a cylinder block in an axial piston pump. World Tribology Congress; 2005. p. 223–4.
[23] Bergada JM, Davies DL, Kumar S, Watton J. The effect of oil pressure and temperature on barrel film thickness and barrel dynamics of an axial piston pump. Meccanica 2012;47(3):639–54.
[24] Kazama T, Tsuruno T. Thermal lubrication characteristics of swash-plate type axial piston pumps (temperature measurement of swash-plate and cylinder-block):temperature measurement of swash-plate and cylinder-block. Trans. Jpn. Soc. Mech. Eng. 2008;74(738):425–30.
[25] Rybicki EF, Strenkowski JS, Tamm MA. A finite element model for compliant bearing lubrication using a minimization algorithm. Wear 1978;47(2):279–92.
[26] Mucchi E, Agazzi A, D'Elia G. On the wear and lubrication regime in variable displacement vane pumps. Wear 2013;306(1–2):36–46.
[27] Park IK, Rhim YC. A study on the characteristics of volumetric efficiency of an axial piston pump considering piston tilting. KSME Int J 2009;10(1/2):37–42.
[28] Pan HC, Sheng J, Lu Y. Finite difference computation of valve plate fluid film flows in axial piston machines. Int J Mech Sci 1989;31(10):779–91.
[29] Zloto T, Kowalski K. Pressure distributions in oil film in the front gap of a hydrostatic thrust bearing vol. 12. Institute of Mechanical Technologies Czestochowa University of Technology; 2012. p. 279–83. 2.
[30] Mostofi A, Gohar R. Oil film thickness and pressure distribution in elasto hydro dynamic point contacts. ARCHIVE J. Mech. Eng. Sci. 1982;24(4):173–82.
[31] Edge KA, Darling J. The pumping dynamics of swash plate piston pumps. J Dyn Syst Meas Contr 1989;111(2):307–12.
[32] Brooks DW. Valve Plate for axial hydraulic piston pump or motor. 2003. US 20030126982 A1.
[33] Nunomura H. High-pressure and low-pressure selecting valve and swash-plate type hydraulic motor system. 2004. US 20040000142 A1.
[34] Zloto T, Sochacki D. Impact of exploitation parameters on the hydrostatic relief of the cylinder block in an axial piston pump vol. 12. 2012. p. 285–90. 2.
[35] Zloto T, Sochacki D, Stryjewski P. Analysis of oil leaks in a variable-height gap between the cylinder block and the valve plate in a piston pump by means of author-designed software and CFD fluent. Nihon Naibunpi Gakkai Zasshi 2014;14(4):211–6.
[36] Hu X, Wang SP, Han L. Modeling and simulation of dynamic pressure distribution of axial piston pump port plate pair. Hydraulics Pneumatics and Seals 2012;32(8):68–71.
[37] Xu B, Sun YH, Zhang JH. A new design method for the transition region of the valve plate for an axial piston pump. J Zhejiang Univ Sci 2015;16(3):229–40.
[38] Kim JK, Jung JY. Measurement of fluid film thickness on the valve plate in oil hydraulic axial piston pumps (I)-Bearing pad effects. KSME Int J 2003;17(2):246–53.
[39] Kim JK, Kim HE, Lee YB. Measurement of fluid film thickness on the valve plate in oil hydraulic axial piston pumps (Part II: spherical design effects). J Mech Sci Technol 2005;19(2):655–63.
[40] Ai QL, Zhou H, Yang HY. Numerical analysis of lubrication property for port plate pair of axial piston pump. Trans Chin Soc Agric Mach 2004;35(6):78–81.
[41] Wang Z, Gu L, Li L. Experimental studies on the overall efficiency performance of axial piston motor with a laser surface textured valve plate. Proc IME B J Eng Manufact 2013;227(7):1049–56.